External-Shell Oxygen Enabling the Local Environment Modulation of Unsaturated NbN 3 for Efficient Electrosynthesis of Hydrogen Peroxide

Dingding Li, Run-Xi Zhu, Zheng Han, Lei Bai, Jianting Zhang, Ruixin Xu, Weilong Ma, Liangpeng Nie, Yi Wang, Jinbo Bai, et al.

External-Shell Oxygen Enabling Local Environment Modulation of Unsaturated NbN_3 for Efficient Electrosynthesis of Hydrogen Peroxide

Dingding Li,[a] Run-Xi Zhu,[b] Zheng Han,[a] Lei Bai,[a] Jianting Zhang,[a] Ruixin Xu,[d] Weilong Ma,[a] Liangpeng Nie,[a] Yi Wang,[a] Jinbo Bai,[c] Hang Zhao,[a] Ji-Quan Liu,[d] Kunyue Leng,[a] Ya-Qiong Su*[b] and Yunteng Qu *[a]*

[a]State Key Laboratory of Photoelectric Technology and Functional Materials, International Collaborative Center on Photoelectric Technology and Nano Functional Materials, Institute of Photonics & Photon-Technology, Northwest University, Xi'an, 710069, PR China.

[b]School of Chemistry, Xi'an Key Laboratory of Sustainable Energy Materials Chemistry, State Key Laboratory of Electrical Insulation and Power Equipment, Xi'an Jiaotong University, Xi'an 710049, PR China.

[c]Université Paris-Saclay, CentraleSupélec, ENS Paris-Saclay, CNRS, LMPS-Laboratoire de Mécanique Paris-Saclay, 8-10 rue Joliot-Curie, Gif-sur-Yvette 91190, France

[d]Key Laboratory of Synthetic and Natural Functional Molecule Chemistry, College of Chemistry & Materials Science, Northwest University, 1 Xuefu Ave., Xi'an 710127, PR China

KEYWORDS: electrocatalysis, Nb single atom, coordination environment regulation, oxygen reduction reaction

ABSTRACT: Single atom catalysts with tunable coordination structure have shown grand potential in flexibly altering the selectivity of oxygen reduction reaction (ORR) towards desired pathway. However, the local coordination number modulation on the single metal sites, which could mediate the ORR pathway, still remains challenging. Herein, we prepare the Nb single atom catalysts (SACs) with external-shell oxygen modulated unsaturated NbN_3 site in carbon nitride and NbN_4 site anchored in nitrogen doped carbon carriers, respectively. Compared with typical NbN_4 moieties for $4e^-$ ORR, the as prepared NbN_3 SACs exhibits excellent $2e^-$ ORR activity in 0.1 M KOH, of which the onset overpotential close to zero (9 mV) and the H_2O_2 selectivity surpass 95%, making it one of the state-of-the-art catalysts in electrosynthesis of hydrogen peroxide. DFT theoretical calculations indicate the unsaturated Nb-N_3 moieties and adjacent oxygen groups optimize the interface bond strength of pivotal intermediates (OOH*) for producing H_2O_2, thus accelerating $2e^-$ ORR pathway. Our findings may provide novel platform for developing SACs with high activity and tunable selectivity.

1. Introduction

Hydrogen peroxide (H_2O_2), as a kind of green oxidant, is widely utilized in the chemical industry, environmental treatment and pharmaceutical manufacturing.[1, 2] Compared to the industrial anthraquinone process with intensive energy consumption and pollution issues, the electrochemical synthesis of H_2O_2 manifests itself as a ideal alternative because of the mild reaction conditions, the exploitation of renewable electricity and green precursors (water and air) as feedstocks.[3-5] Various noble metals catalysts, such as Pd-Au,[6] Pd-Hg,[7] Au-Pt-Ni[8] and PtP_2[9], have been demonstrated efficient for $2e^-$ oxygen reduction reaction (ORR), but their scarcity and high cost significantly hinder the practical application in industry.[10] In this context, developing

efficient and substitutive non-noble based electrocatalysts that could enable high H_2O_2 selectivity at a relative low reaction barrier of is of great importance.

An ideal $2e^-$ ORR electrocatalyst demands neither too strong nor too weak bonding strength between active sites and oxygen species for preservation of O-O bond.[11, 12] Therefore, a catalyst platform with flexibly tailorable electronic structure is crucial for modulating the ORR pathway and boosting the desired kinetic process. [13, 14] Thanks to the maximum atomic utilization and adjustable coordination structure, single-atom catalysts (SACs) may provide a promising platform to flexibly manipulate the ORR pathway.[15-17] Recently, it has been demonstrated that introducing heteroatom doping (O, B, S, P, etc.) into Fe/Co/Ni-N-C single metal site can engineer the local environment of single metal active site for desired $2e^-$ ORR.[3, 18-21] However, these heteroatom doping strategies cause the problems of demetallation and stability issues of single metal sites at harsh operating conditions.[22, 23] Even worse, the dissociative metal ions, especially iron and cobalt ions, will potentially lead to the decomposition of H_2O_2 due to Fenton effect. Different from heteroatom doping strategy, tailoring the coordination number of M-N sites offers another intriguing approach to simultaneously regulate the electronic structure and maintain the robust stability of SACs.[24, 25] Actually, it is found that engineering local coordination number of atomically dispersed M-N_x moieties can greatly promote the reaction activity.[26-28] However, the local coordination number modulation on the metal-N sites, which could mediate the $2e^-$/$4e^-$ ORR pathways, still remains challenging and has rarely been investigated.

In this work, we rationally modulate the coordination number of single Nb-N sites and external-shell oxygen group to tailor ORR pathway. Inspired by CNT composites based on multiple types of structures,[29, 30] the as-prepared catalyst possesses an unsaturated Nb-N_3

configuration in graphitic carbon nitride on carbon nanotubes and the oxygen group species on second coordination carbon, which is denoted as NbN_3-(O)C_3N_4/OCNT. Compared with typical NbN_4/NC orienting to $4e^-$ ORR pathway, NbN_3-(O)C_3N_4/OCNT exhibits excellent $2e^-$ ORR activity with a near zero overpotential, a H_2O_2 selectivity over 95%, as well as superior H_2O_2 productivity (1020.4 mmol $g_{catalyst}^{-1}$ h^{-1} at 0 V) in flow cell, make it one of the state-of-the-art catalysts in electrosynthesis of hydrogen peroxide. DFT theoretical calculations in combination with control experiments indicate the unsaturated Nb-N_3 moieties and external-shell oxygen group regulate electron distribution around Nb sites, thus optimizing the adsorption/desorption strength of pivotal reaction intermediates (*OOH) for producing H_2O_2.

2. Results and Discussion

2.1. Synthesis and structural characterizations of NbN_3-(O)C_3N_4/OCNT

NbN_3-(O)C_3N_4/OCNT was prepared by a typical impregnation-pyrolysis strategy, in which the thermal pyrolysis of dicyanamide, niobium oxalate and oxidized carbon nanotube (OCNT) conducted at 600 °C (Figure 1a). For comparison, NbN_3-C_3N_4/CNT and NbN_4/NC were also prepared through similar methods (Figure S1). SEM and TEM images uncovered the resultant NbN_3-(O)C_3N_4/OCNT took the similar morphology with CNT (Figure S2). Moreover, a thin layer of g-C_3N_4 enveloped on the OCNT is observed at HRTEM image (Figure 1b). Furthermore, the N1s XPS analysis (Figure S3) and the larger specific surface areas of NbN_3-(O)C_3N_4/OCNT

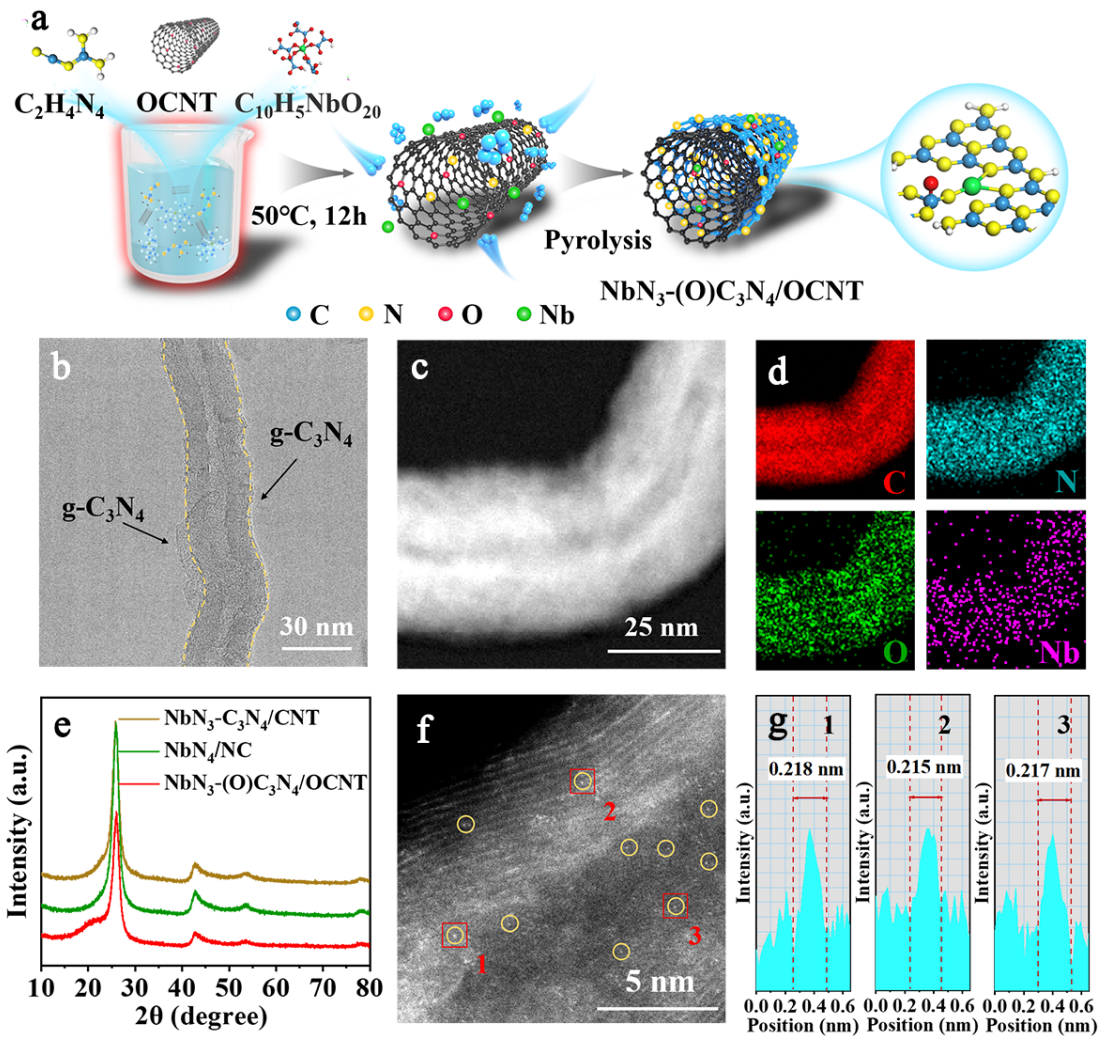

Figure 1. Synthesis and characterizations. (a) Schematic diagram for the preparing of NbN_3-(O)C_3N_4/OCNT. (b) TEM image, (c) HAADF-STEM image, (d) EDS mappings of NbN_3-(O)C_3N_4/OCNT. (e) XRD patterns of NbN_3-C_3N_4/CNT, NbN_4/NC and NbN_3-(O)C_3N_4/OCNT. (f) Aberration-corrected HAADF-STEM image of NbN_3-(O)C_3N_4/OCNT. (g) Intensity profiles obtained from the area highlighted with red box in f.

(146.8 m^2/g) than that of OCNT (134.5 m^2/g) further indicated the formation of C_3N_4 layer (Figure S4 and Table S1). The HAADF-STEM image and corresponding EDS element mapping demonstrated the existence and homogeneous dispersion of Nb elenmet, no obvious Nb particles was observed (Figure 1c and d). The XRD parttern of NbN_3-(O)C_3N_4/OCNT exhibited only the diffraction peaks belong to C_3N_4/OCNT, further demonstrating the poor crystallinity of Nb

(Figure S5). The atomic distribution of Nb sites in the as-prepared catalyst is distinguished by Aberration-corrected HAADF-STEM. 1f and g, bright spots with diameter around 0.22 nm were randomly dispersed on C_3N_4 enveloped OCNT, indicating the existence of atomic dispersed Nb sites on NbN_3-$(O)C_3N_4$/OCNT. The Nb content was confirmed to 0.21 wt% by ICP-OES (Table S1). The NbN_3-C_3N_4/CNT and NbN_4/NC with atomically dispersed Nb sites were also demonstrated by XRD (Figure 1e) and HAADF-STEM (Figure S6 and S7).

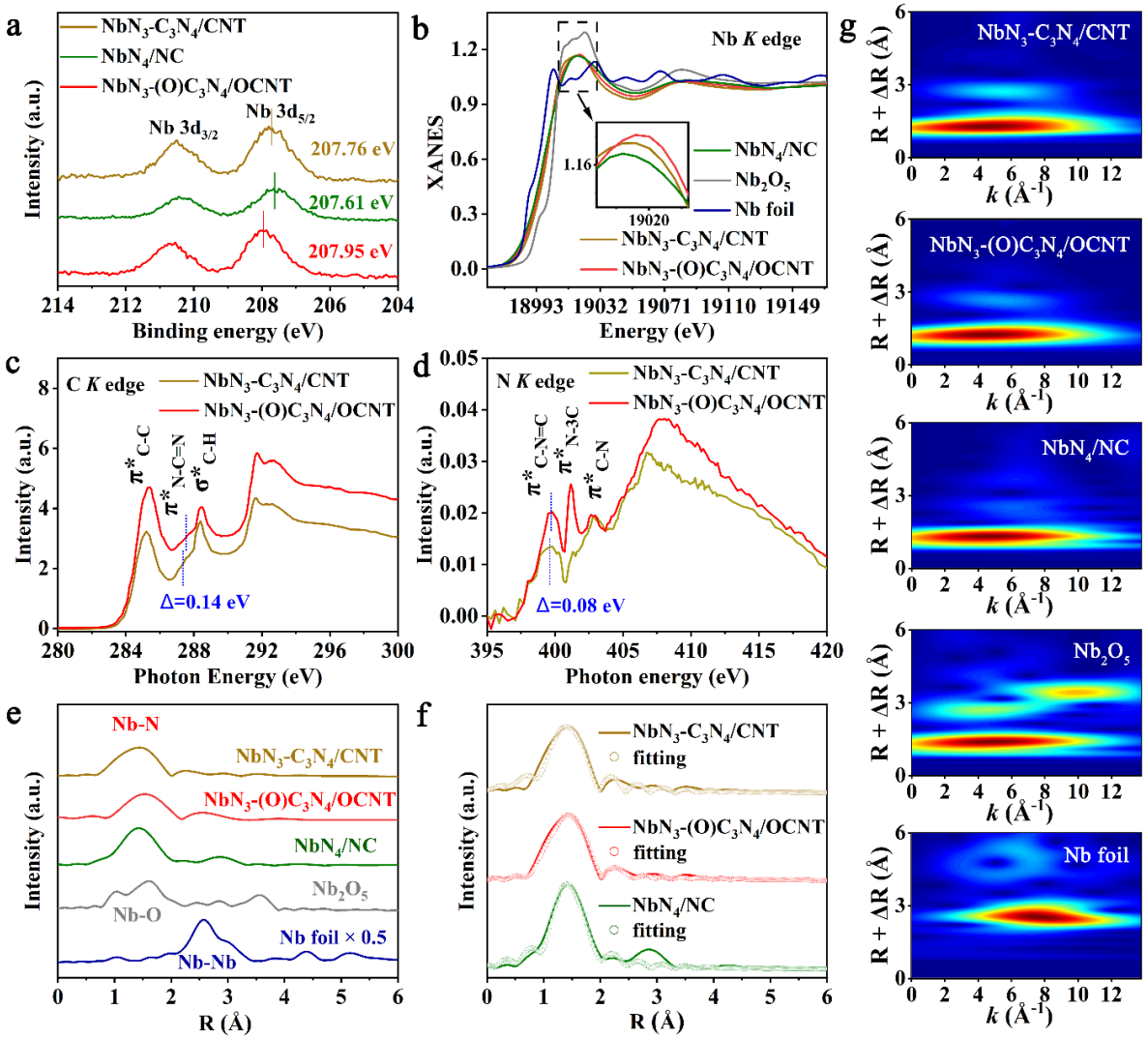

Figure 2. (**a**) Nb 3d XPS spectrum and (**b**) Nb K edge X-ray absorption near-edge spectroscopy spectra of NbN_3-$(O)C_3N_4$/OCNT and the reference samples. (**c**) C K edge and (**d**) N K edge XANES spectra of NbN_3-$(O)C_3N_4$/OCNT and NbN_3-C_3N_4/CNT. (**e**) FT-EXAFS spectra and (**f**) EXAFS fitting curves of NbN_3-$(O)C_3N_4$/OCNT and the reference samples. (**g**) Continuously

Cauchy wavelet transform k^3-weighted EXAFS spectra of NbN_3-$(O)C_3N_4$/OCNT and the reference samples.

Furthermore, X-ray photoelectron spectroscopy (XPS) and X-ray absorption spectroscopy (XAS) were adopted to clarify the coordination environment and electronic state of Nb SACs. The N 1s spectra analysis showed the existent of Nb-N bonding on NbN_3-$(O)C_3N_4$/OCNT, NbN_3-C_3N_4/CNT and NbN_4/NC (Figure S8). The peaks of Nb 3d spectra for NbN_3-$(O)C_3N_4$/OCNT, NbN_3-C_3N_4/CNT and NbN_4/NC can be examined at 207.9, 207.7 and 207.6 eV, respectively, which located between Nb^0 and Nb^{5+} (Figure 2a). This observation demonstrated the partially positive oxidative state of $Nb^{\delta+}$ ($0<\delta<5$) in Nb SACs. Based on the Nb K edge XANES spectra (Figure 2b), the white-line intensity of NbN_3-$(O)C_3N_4$/OCNT, NbN_3-C_3N_4/CNT and NbN_4/NC located between Nb foil and Nb_2O_5, in line with the Nb 3d XPS results. Notably, the single Nb sites in NbN_3-$(O)C_3N_4$/OCNT exhibited unique electronic structure, as demonstrated by the higher oxidative state of Nb in NbN_3-$(O)C_3N_4$/OCNT than those of NbN_3-C_3N_4/CNT and NbN_4/NC. The lower oxidative state of Nb in NbN_4/NC may be ascribed to different coordination number of Nb-N. On the other hand, the difference in oxidative state of Nb between NbN_3-$(O)C_3N_4$/OCNT and NbN_3-C_3N_4/CNT may be due to the oxygen group species on CNT. For further elucidating the effect of O group, C K edge and N K edge XANES spectra were measured over NbN_3-$(O)C_3N_4$/OCNT and NbN_3-C_3N_4/CNT, respectively. It can be seen from the C K edge XANES spectra (Figure 2c), compared with NbN_3-C_3N_4/CNT, the peak of $\pi^*_{N\text{-}C=N}$ attributed to C_3N_4 showed a significant positive shift (0.14 eV) on NbN_3-$(O)C_3N_4$/OCNT. Meanwhile, the slight shift towards higher energy areas (0.08 eV) also can be observed in $\pi^*_{C\text{-}N=C}$ based on the N K edge XANES spectra (Figure 2d). Together, the stronger charge transfer occurred on C atoms of C_3N_4, indicating that O species were proposed to bond with second coordination carbon sites. As depicted in Figure 2e, the EXAFS at R-space showed

only a dominant peak at ~1.5 Å assigned to Nb-N bonding for these Nb samples. Additionally, the absence of Nb-Nb bonding at ~2.6 Å and wavelet transform k^3-weighted EXAFS spectra (Figure 2g) suggested the atomically dispersed of Nb species in the three as-obtained samples. According to corresponding fitting results at R-space (Figure 2f), NbN_3-(O)C_3N_4/OCNT and NbN_3-C_3N_4/CNT displayed the NbN_3 coordination structure, while NbN_4/NC exhibited the NbN_4 coordination structure (Figure S9 and Table S2), consistent with XPS analysis. And these results above provided solid evidence for successfully fabricating Nb SACs.

2.2. Electrochemical Oxygen Reduction Reaction

The as-prepared Nb SACs feature unique metal center and tunable electron structure, which provides potential opportunity to modulate the activity and selectivity for electrocatalysis. Thus, their ability to drive and alter the ORR pathway was evaluated in 0.1 M KOH with a catalyst loading of 0.10 mg cm^{-2}. As exhibited in Figure 3a and Figure S10, the OCNT-based NbN_3 catalyst, NbN_3-(O)C_3N_4/OCNT, showed a superior onset potential of 0.816 V (at -0.1 mA cm^{-2}, vs RHE), which approached the theoretical limit for $2e^-$ ORR (0.825 V vs RHE).[31] The fast ORR kinetics of NbN_3-(O)C_3N_4/OCNT was also confirmed by a low Tafel slope of 70.5 mV dec^{-1} (Figure S11). The selectivity towards H_2O_2 was calculated by rotating ring-disk electrode (RRDE) tests. The NbN_3-(O)C_3N_4/OCNT delivered a high H_2O_2 selectivity with 95% and a nearly 2 electron transfer (n=2.07) at a wide potential window (0.4-0.7 V vs RHE) (Figure 3b and Figure S12), outperforming most reported catalysts for $2e^-$ ORR in alkaline media (Figure 3c). Conversely, the CNT-based catalysts, NbN_3-C_3N_4/CNT (59.5%) and NbN_4/NC (27.4%) were more favorable to approach the $4e^-$ ORR. This observation indicated the unsaturated NbN_3 coordination and the oxygen species around Nb sites provided by the functionalized OCNT play important role to optimize the electronic structure of Nb SACs, hence altering ORR pathway. Furthermore, the CNT and OCNT also exhibited poor selectivity for $2e^-$ ORR (16.5% and

18.4%), which excluded the possible contribution of supports. And the higher selectivity of C_3N_4/OCNT (22.3%) compared with OCNT suggests that C_3N_4 favors ORR pathway shift.

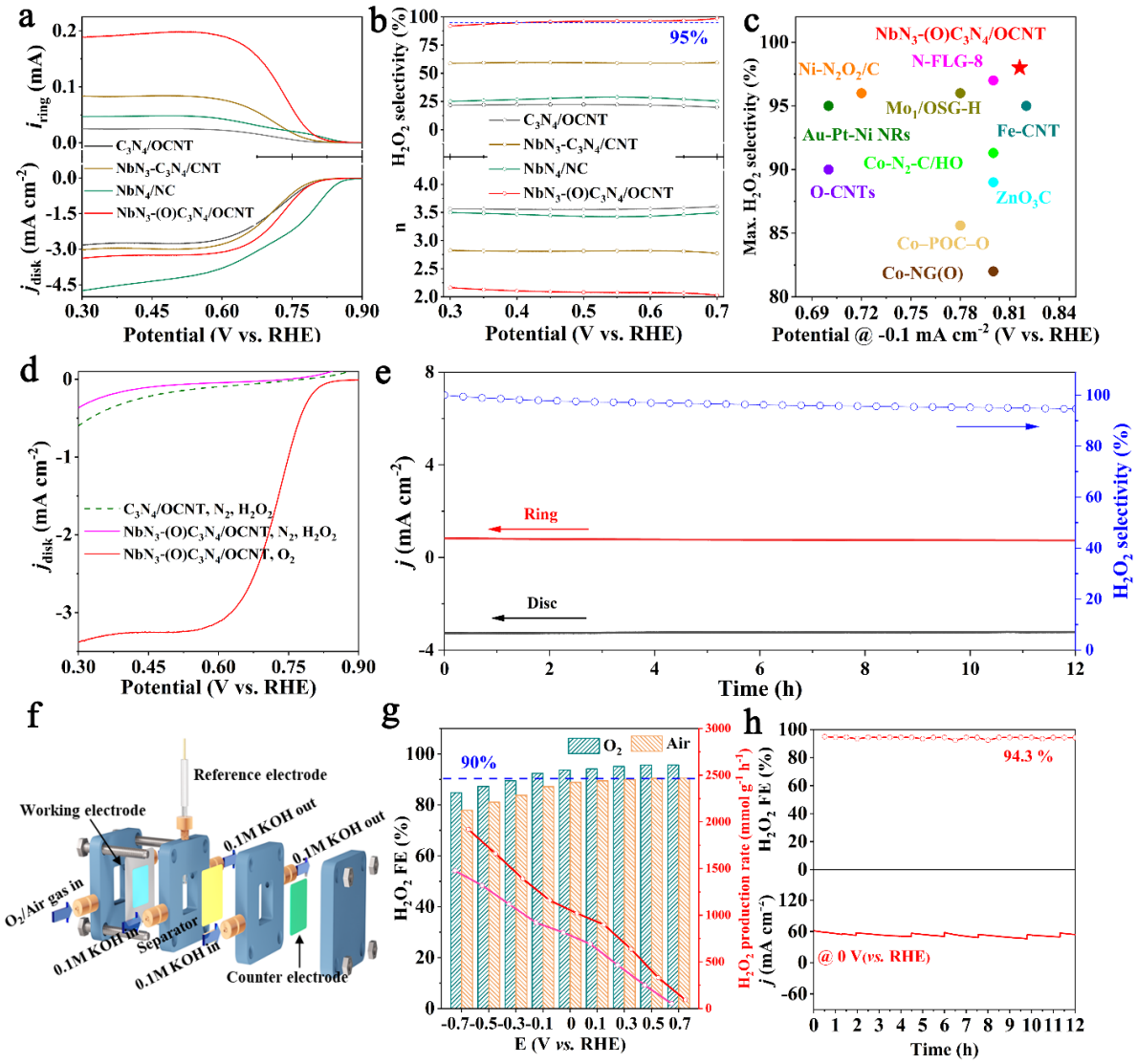

Figure 3 Electrochemical ORR evaluation. (**a**) RRDE voltammograms obtained in O_2-saturated 0.1 M KOH with disk current density (j_{disk}) and the ring currents (i_{ring}). (**b**) Calculated H_2O_2 selectivity and electron transfer number (n) from RRDE. (**c**) Comparison of the onset potential and maximum H_2O_2 selectivity on NbN_3-(O)C_3N_4/OCNT and other reported electrocatalysts. (**d**) Voltammograms for NbN_3-(O)C_3N_4/OCNT obtained in 0.1 M KOH containing 10 mm H_2O_2. (**e**) Stability measurement of NbN_3-(O)C_3N_4/OCNT at a fixed disk potential of 0.5 V versus RHE. (**f**) Schematic illustration of the flow cell electrolytic device. (**g**)

The corresponding H_2O_2 selectivity and production rate in the flow cell with different feed gas. (**h**) Long-term stability test of NbN_3-$(O)C_3N_4$/OCNT at 0 V (versus RHE) and corresponding H_2O_2 FE in flow cell.

For evaluating the stability of H_2O_2 at operating conditions, the electrochemical H_2O_2 reduction testing was conducted in N_2-saturated 0.1 M KOH adding 10 mM hydrogen peroxide. Figure 3d showed that the NbN_3-$(O)C_3N_4$/OCNT achieved an insignificant reaction current, verifying the poor activity for H_2O_2 reduction. The robust stability of NbN_3-$(O)C_3N_4$/OCNT was revealed by the chronoamperometric test at a constant disk potential of 0.5 V. After continuous operating for 12 h, the H_2O_2 selectivity still retained over 95% (Figure 3e). Moreover, we performed the post-catalysis SEM, TEM, XRD and HAADF-STEM (Figure S13) and demonstrated the stability of NbN_3 sites on NbN_3-$(O)C_3N_4$/OCNT.

Inspired by the superior activity and selectivity of NbN_3-$(O)C_3N_4$/OCNT in three-electrode system, a flow cell system was assembled to simulate the scale-up H_2O_2 using pure O_2 and air. As shown in Figure 3f, cathode was obtained by attaching NbN_3-$(O)C_3N_4$/OCNT on gas diffusion layer (1 mg cm^{-2}) and the iridium oxide was used as the anode. The produced H_2O_2 was analyzed by the cerium sulfate titration method (Figure S14 and S15). The LSV curves showed the reaction current density can reach -135 mA cm^{-2} and -110 mA cm^{-2} (at -0.8 V) under O_2 and air flow, respectively (Figure S16). As shown in Figure 3g, NbN_3-$(O)C_3N_4$/OCNT exhibited a high Faraday efficiency for H_2O_2 production over 90% from -0.1 to 0.7V. Particularly, an excellent H_2O_2 production rate was gained 1020.4 mmol $g_{catalyst}^{-1}$ h^{-1} over NbN_3-$(O)C_3N_4$/OCNT at 0 V, which surpassed most reported $2e^-$ ORR electrocatalysts (Table S3). Moreover, when the flow gas was change to air, just a slight decay of H_2O_2 production was observed. Chronopotentiometry measurement uncovered that H_2O_2 could be continuously and efficiently produced for 12 h in O_2 or air flow (Figure 3h and Figure S17). Together, these results above

demonstrate the excellent activity of NbN_3-$(O)C_3N_4$/OCNT for H_2O_2 electrosynthesis and display promising prospect in scaling up H_2O_2 towards the industrial application.

2.3. Operando Electrochemical Raman and DFT Calculations

To further investigated the regulation of ORR pathway over NbN_3 sites, electrochemical operando Raman spectra of NbN_3-$(O)C_3N_4$/OCNT and NbN_4/NC were measured in O_2-saturated 0.1 M KOH (Figure S18). It can be seen in Figure 4a, no extra signal was detected at 1 V over neither NbN_4/NC nor NbN_3-$(O)C_3N_4$/OCNT, due the insufficient dynamics. After negatively shifting the applied potential to 0.6 V, a strong band belong to *OOH species, as a commonly intermediate in $2e^-$ ORR pathway, emerged at 840.7 cm^{-1} on NbN_3-$(O)C_3N_4$/OCNT.[32] However, for NbN_4/NC the band at 840.7 cm^{-1} is quite weak and an obviously new signal belong to *OH at emerged at 1088.2 cm^{-1},[33] indicating the NbN_4/NC is more favorable to decompose *OOH species to trigger $4e^-$ ORR pathway. The above results demonstrated that superior 2 e^- ORR performance of NbN_3-$(O)C_3N_4$/OCNT stem from its modest interaction between reaction intermediate, which boosted the ORR dynamics without decomposing *OOH species into *OH.

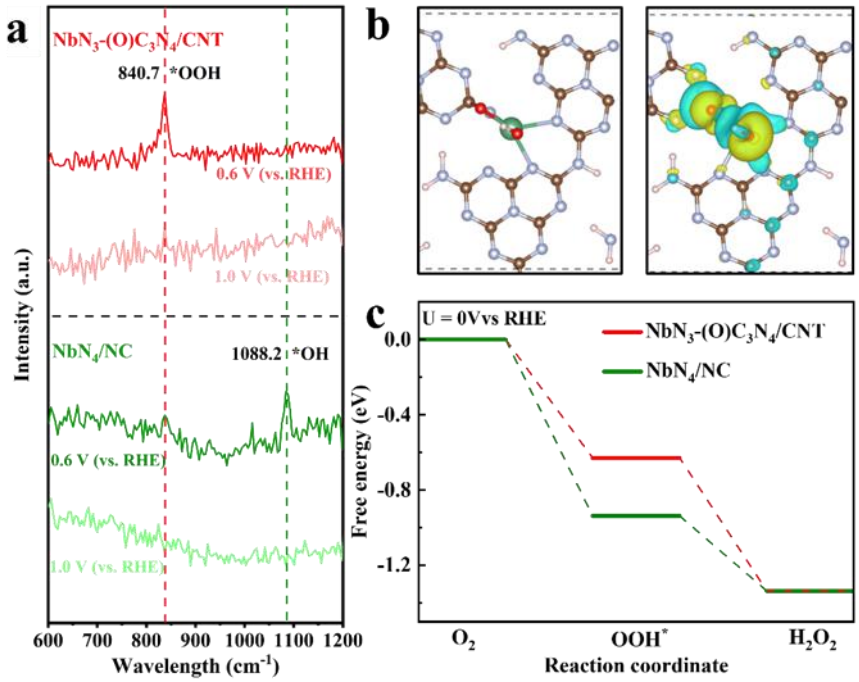

Figure 4 (**a**) Electrochemical operando Raman spectra recorded in O_2-saturated 0.10 M KOH. (**b**) Free energy diagram of $2e^-$ ORR on NbN_3-$(O)C_3N_4$/OCNT and NbN_4/NC at 0 V vs. RHE. (**c**) Charge density differences of NbN_3-$(O)C_3N_4$/OCNT and NbN_4/NC.

Density functional theory (DFT) calculations further disclose the effect of Nb coordination environment on the $2e^-$ ORR pathway. Figure 4b displays the free-energy evolution diagram of NbN_3-$(O)C_3N_4$/OCNT and NbN_4/NC. The potential-determining step of NbN_3-$(O)C_3N_4$/OCNT is the first-step that reducing O_2 to form the *OOH species, resulting in an overpotential of 0.039 eV. While the potential-determining step of NbN_4/NC is the second-step reduction of *OOH to form H_2O_2 intermediate with an overpotential of 0.27 eV. Demonstrating the more efficient 2 e^- ORR dynamics over NbN_3-$(O)C_3N_4$/OCNT, which in good agreement with its rational charge distribution between Nb-N sites and O-containing species (Figure 4c).

3. Conclusion

In summary, we synthesized NbN_3-$(O)C_3N_4$/OCNT by modulating the coordination number of single Nb-N site and adjacent oxygen groups, and applied it to H_2O_2 electrosynthesis.

Compared with NbN_4/NC with saturated nitrogen coordination, the NbN_3-$(O)C_3N_4$/OCNT electrocatalyst with unsaturated Nb-N_3 moieties exhibits excellent catalytic performance for $2e^-$ ORR pathway, with a near zero overpotential, a H_2O_2 selectivity over 95%, as well as superior H_2O_2 productivity (1020.4 mmol $g_{catalyst}^{-1}$ h^{-1} at 0 V) in flow cell. DFT theoretical calculations in combination with in situ Raman spectroscopy indicate the unsaturated Nb-N_3 moieties and adjacent oxygen group regulate electron distribution around Nb sites, thus optimizing the adsorption/desorption strength of pivotal reaction intermediates (*OOH) for producing H_2O_2. It can be expected that this work will provide more options for future catalyst design and its coordination control.

ASSOCIATED CONTENT

Supporting Information

This material is available free of charge via the Internet at http://pubs.acs.org.

Experimental Section, Electrochemical measurements, Computational Method and Characterizations.

AUTHOR INFORMATION

Corresponding Authors

*__Kunyue Leng__ − State Key Laboratory of Photoelectric Technology and Functional Materials, International Collaborative Center on Photoe-lectric Technology and Nano Functional Materials, Institute of Photonics & Photon-Technology, Northwest University, Xi'an, 710069, PR China
Email: lengky@nwu.edu.cn

*__Ya-Qiong Su__ − School of Chemistry, Xi'an Key Laboratory of Sustainable Energy Materials Chemistry, State Key Laboratory of Electrical Insulation and Power Equipment, Xi'an Jiaotong University, Xi'an 710049, China
Email: yqsu1989@xjtu.edu.cn

Yunteng Qu − State Key Laboratory of Photoelectric Technology and Functional Materials, International Collaborative Center on Photoe-lectric Technology and Nano Functional Materials, Institute of Photonics & Photon-Technology, Northwest University, Xi'an, 710069, PR China
Email: yuntengqu@nwu.deu.cn

Authors

Dingding Li − State Key Laboratory of Photoelectric Technology and Functional Materials, International Collaborative Center on Photoe-lectric Technology and Nano Functional Materials, Institute of Photonics & Photon-Technology, Northwest University, Xi'an, 710069, PR China

Run-Xi Zhu − School of Chemistry, Xi'an Key Laboratory of Sustainable Energy Materials Chemistry, State Key Laboratory of Electrical Insulation and Power Equipment, Xi'an Jiaotong University, Xi'an 710049, China

Zheng Han − State Key Laboratory of Photoelectric Technology and Functional Materials, International Collaborative Center on Photoe-lectric Technology and Nano Functional Materials, Institute of Photonics & Photon-Technology, Northwest University, Xi'an, 710069, PR China

Lei Bai − State Key Laboratory of Photoelectric Technology and Functional Materials, International Collaborative Center on Photoe-lectric Technology and Nano Functional Materials, Institute of Photonics & Photon-Technology, Northwest University, Xi'an, 710069, PR China

Jianting Zhang − State Key Laboratory of Photoelectric Technology and Functional Materials, International Collaborative Center on Photoe-lectric Technology and Nano Functional Materials, Institute of Photonics & Photon-Technology, Northwest University, Xi'an, 710069, PR China

Ruixin Xu − Key Laboratory of Synthetic and Natural Functional Molecule Chemistry, College of Chemistry & Materials Science, Northwest University, 1 Xuefu Ave., Xi'an 710127, PR China

Weilong Ma − State Key Laboratory of Photoelectric Technology and Functional Materials, International Collaborative Center on Photoe-lectric Technology and Nano Functional Materials, Institute of Photonics & Photon-Technology, Northwest University, Xi'an, 710069, PR China

Liangpeng Nie − State Key Laboratory of Photoelectric Technology and Functional Materials, International Collaborative Center on Photoe-lectric Technology and Nano Functional Materials, Institute of Photonics & Photon-Technology, Northwest University, Xi'an, 710069, PR China

Yi Wang − State Key Laboratory of Photoelectric Technology and Functional Materials, International Collaborative Center on Photoe-lectric Technology and Nano Functional Materials, Institute of Photonics & Photon-Technology, Northwest University, Xi'an, 710069, PR China
Jinbo Bai − Université Paris-Saclay, CentraleSupélec, ENS Paris-Saclay, CNRS, LMPS-Laboratoire de Mécanique Paris-Saclay, 8-10 rue Joliot-Curie, Gif-sur-Yvette 91190, France
Hang Zhao − State Key Laboratory of Photoelectric Technology and Functional Materials, International Collaborative Center on Photoe-lectric Technology and Nano Functional Materials, Institute of Photonics & Photon-Technology, Northwest University, Xi'an, 710069, PR China
Ji-Quan Liu − Key Laboratory of Synthetic and Natural Functional Molecule Chemistry, College of Chemistry & Materials Science, Northwest University, 1 Xuefu Ave., Xi'an 710127, PR China

Author Contributions

K.L. and Y.Q. conceptualized and co-wrote this work. Y.S. designed and supervised the DFT calculations. D.L. synthesized the catalysts and carried out the electrochemistry evaluation. R.Z. carried out the DFT calculations. Z.H., L.B., J.Z., R.X., W.M., L.N. helped arrange the material characterizations. Y.W., J.B., H.Z., and J.-Q.L. helped with modification of the paper. All authors discussed and revised the manuscript.

Funding

This work was financially supported by the National Natural Science Foundation of China (21902150), Natural Science Basic Research Program of Shaanxi (2022JQ-082 and 2022JM-018) and China Postdoctoral Science Foundation (2020M673461 and 2021M692609).

Notes

The authors declare no competing financial interest.

ACKNOWLEDGMENT

This work is financially supported by the National Natural Science Foundation of China (21902150), Natural Science Basic Research Program of Shaanxi (2022JQ-082 and 2022JM-018) and China Postdoctoral Science Foundation (2020M673461 and 2021M692609). Y. Su acknowledge the "Young Talent Support Plan" of Xi'an Jiaotong University. Supercomputing facilities were provided by Hefei Advanced Computing Center. We thank the photoemission endstation beamline 1W1B station in the Beijing Synchrotron Radiation Facility (BSRF), BL14W1 in Shanghai Synchrotron Radiation Facility (SSRF), BL10B and BL11U in National Synchrotron Radiation Laboratory (NSRL) for the help in characterizations.

REFERENCES

(1) Perry, S. C.; Pangotra, D.; Vieira, L.; Csepei, L.-I.; Sieber, V.; Wang, L.; Ponce de León, C.; Walsh, F. C., Electrochemical synthesis of hydrogen peroxide from water and oxygen. *Nat. Rev. Chem.* **2019,** *3*, 442-458.
(2) Campos‐Martin, J. M.; Blanco-Brieva, G.; Fierro, J. L., Hydrogen peroxide synthesis: an outlook beyond the anthraquinone process. *Angew. Chem. Int. Ed.* **2006,** *45*, 6962-6984.
(3) Li, B. Q.; Zhao, C. X.; Liu, J. N.; Zhang, Q., Electrosynthesis of hydrogen peroxide synergistically catalyzed by atomic Co-Nx-C sites and oxygen functional groups in noble-metal-free electrocatalysts. *Adv. Mater.* **2019,** *31*, 1808173.
(4) Jiang, K.; Back, S.; Akey, A. J.; Xia, C.; Hu, Y.; Liang, W.; Schaak, D.; Stavitski, E.; Nørskov, J. K.; Siahrostami, S., Highly selective oxygen reduction to hydrogen peroxide on transition metal single atom coordination. *Nat. Commun.* **2019,** *10*, 1-11.
(5) Wu, G.; More, K. L.; Johnston, C. M.; Zelenay, P., High-performance electrocatalysts for oxygen reduction derived from polyaniline, iron, and cobalt. *Science* **2011,** *332*, 443-447.
(6) Pizzutilo, E.; Kasian, O.; Choi, C. H.; Cherevko, S.; Hutchings, G. J.; Mayrhofer, K.; Freakley, S. J., Electrocatalytic synthesis of hydrogen peroxide on Au-Pd nanoparticles: From fundamentals to continuous production. *Chem. Phys. Lett.* **2017,** *683*, 436-442.
(7) Samira; Siahrostami; Arnau; Verdaguer-Casadevall; Mohammadreza; Karamad, Enabling direct H_2O_2 production through rational electrocatalyst design. *Nat. Mater.* **2013,** *12*, 1137-1143.
(8) Zheng, Z.; Ng, Y. H.; Wang, D. W.; Amal, R., Epitaxial growth of Au-Pt-Ni nanorods for direct high selectivity H_2O_2 production. *Adv. Mater.* **2016,** *28*, 9949-9955.
(9) Li, H.; Wen, P.; Itanze, D. S.; Hood, Z. D.; Adhikari, S.; Lu, C.; Ma, X.; Dun, C.; Jiang, L.; Carroll, D. L. Scalable neutral H_2O_2 electrosynthesis by platinum diphosphide nanocrystals by regulating oxygen reduction reaction pathways. *Nat. Commun.* **2020,** *11*, 1-12.
(10) Zhu, W.; Chen, S., Recent Progress of Single-atom Catalysts in the Electrocatalytic Reduction of Oxygen to Hydrogen Peroxide. *Electroanalysis* **2020,** *32*, 2591-2602.
(11) Kulkarni, A.; Siahrostami, S.; Patel, A.; Nørskov, J. K., Understanding catalytic activity trends in the oxygen reduction reaction. *Chem. Rev.* **2018,** *118*, 2302-2312.
(12) San Roman, D.; Krishnamurthy, D.; Garg, R.; Hafiz, H.; Lamparski, M.; Nuhfer, N. T.; Meunier, V.; Viswanathan, V.; Cohen-Karni, T., Engineering three-dimensional (3D) out-of-plane graphene edge sites for highly selective two-electron oxygen reduction electrocatalysis. *ACS Catal.* **2020,** *10*, 1993-2008.

(13) Yaling, J.; Xue, Z.; Yang, J.; Liu, Q.; Xian, J.; Zhong, Y.; Sun, Y.; Zhang, X.; Yao, D.; Li, G., Tailoring the Electronic Structure of Atomically Dispersed Zn Electrocatalyst by Coordination Environment Regulation for High Selectivity Oxygen Reduction. *Angew. Chem. Int. Ed.* **2022,** *61*, e202110838.
(14) Wei, X.; Luo, X.; Wu, N.; Gu, W.; Lin, Y.; Zhu, C., Recent advances in synergistically enhanced single-atomic site catalysts for boosted oxygen reduction reaction. *Nano Energy* **2021,** *84*, 105817.
(15) Liu, X.; Zheng, L.; Han, C.; Zong, H.; Yang, G.; Lin, S.; Kumar, A.; Jadhav, A. R.; Tran, N. Q.; Hwang, Y., Identifying the Activity Origin of a Cobalt Single-Atom Catalyst for Hydrogen Evolution Using Supervised Learning. *Adv. Funct. Mater.* **2021,** *31*, 2100547.
(16) Guo, W.; Wang, Z.; Wang, X.; Wu, Y., General Design Concept for Single-Atom Catalysts toward Heterogeneous Catalysis. *Adv. Mater.* **2021,** *33*, 2004287.
(17) Song, Z.; Zhang, L.; Doyle‐Davis, K.; Fu, X.; Luo, J. L.; Sun, X., Recent advances in MOF-derived single atom catalysts for electrochemical applications. *Adv. Energy Mater.* **2020,** *10*, 2001561.
(18) Wang, Y.; Shi, R.; Shang, L.; Waterhouse, G. I.; Zhao, J.; Zhang, Q.; Gu, L.; Zhang, T., High‐Efficiency Oxygen Reduction to Hydrogen Peroxide Catalyzed by Nickel Single-Atom Catalysts with Tetradentate N_2O_2 Coordination in a Three-Phase Flow Cell. *Angew. Chem. Int. Ed.* **2020,** *59*, 13057-13062.
(19) Gu, W.; Wang, X.; Wen, J.; Cao, S.; Jiao, L.; Wu, Y.; Wei, X.; Zheng, L.; Hu, L.; Zhang, L., Modulating Oxygen Reduction Behaviors on Nickel Single-Atom Catalysts to Probe the Electrochemiluminescence Mechanism at the Atomic Level. *Anal. Chem.* **2021,** *93*, 8663–8670.
(20) Yang, S.; Zhao, C.; Qu, R.; Cheng, Y.; Liu, H.; Huang, X., Probing the activity of transition metal M and heteroatom N_4 co-doped in vacancy fullerene ($M\text{-}N_4\text{-}C_{64}$, M= Fe, Co, and Ni) towards the oxygen reduction reaction by density functional theory. *RSC Adv.* **2021,** *11*, 3174-3182.
(21) Xiao, C.; Cheng, L.; Zhu, Y.; Wang, G.; Chen, L.; Wang, Y.; Chen, R.; Li, Y.; Li, C. J. A. C., Super-Coordinated $N_4\text{-}Ni_1\text{-}O_2$ for Selective H_2O_2 Electrosynthesis at High Current Densities. doi.org/10.1002/ange.202206544
(22) Chen, M.; He, Y.; Spendelow, J. S.; Wu, G., Atomically dispersed metal catalysts for oxygen reduction. *ACS Energy Lett.* **2019,** *4*, 1619-1633.
(23) He, Y.; Liu, S.; Priest, C.; Shi, Q.; Wu, G., Atomically dispersed metal-nitrogen–carbon catalysts for fuel cells: advances in catalyst design, electrode performance, and durability improvement. *Chem. Soc. Rev.* **2020,** *49*, 3484-3524.
(24) Ma, S.; Han, Z.; Leng, K.; Liu, X.; Wang, Y.; Qu, Y.; Bai, J., Ionic Exchange of Metal−Organic Frameworks for Constructing Unsaturated Copper Single-Atom Catalysts for Boosting Oxygen Reduction Reaction. *Small* **2020,** *16*, 2001384.
(25) Feng, J.; Gao, H.; Zheng, L.; Chen, Z.; Zeng, S.; Jiang, C.; Dong, H.; Liu, L.; Zhang, S.; Zhang, X., A Mn-N 3 single-atom catalyst embedded in graphitic carbon nitride for efficient CO 2 electroreduction. *Nat. Commun.* **2020,** *11*, 1-8.
(26) Zhang, F.; Zhu, Y.; Tang, C.; Chen, Y.; Qian, B.; Hu, Z.; Chang, Y. C.; Pao, C. W.; Lin, Q.; Kazemi, S. A., High-Efficiency Electrosynthesis of Hydrogen Peroxide from Oxygen Reduction Enabled by a Tungsten Single Atom Catalyst with Unique Terdentate N_1O_2 Coordination. *Adv. Funct. Mater.* **2022,** *32*, 2110224.

(27) Gong, H.; Wei, Z.; Gong, Z.; Liu, J.; Ye, G.; Yan, M.; Dong, J.; Allen, C.; Liu, J.; Huang, K., Low-Coordinated Co-N-C on Oxygenated Graphene for Efficient Electrocatalytic H_2O_2 Production. *Adv. Funct. Mater.* **2022,** *32*, 2106886.
(28) Jia, B.; Bai, L.; Han, Z.; Li, R.; Huangfu, J.; Li, C.; Zheng, J.; Qu, Y.; Leng, K.; Wang, Y., High-Performance Styrene Epoxidation with Vacancy-Defect Cobalt Single-Atom Catalysts. *ACS Appl. Mater.Interfaces* **2022,** *14*, 10337-10343.
(29) Cortés-Súarez, J.; Celis-Arias, V.; Beltrán, H. I.; Tejeda-Cruz, A.; Ibarra, I. A.; Romero-Ibarra, J. E.; Sánchez-González, E.; Loera-Serna, S., Synthesis and characterization of an SWCNT@ HKUST-1 composite: enhancing the CO_2 adsorption properties of HKUST-1. *ACS omega* **2019,** *4*, 5275-5282.
(30) White, D. L.; Day, B. A.; Zeng, Z.; Schulte, Z. M.; Borland, N. R.; Rosi, N. L.; Wilmer, C. E.; Star, A., Size discrimination of carbohydrates via conductive carbon Nanotube@ Metal organic framework composites. *J. Am. Chem. Soc.* **2021,** *143*, 8022-8033.
(31) Jung, E.; Shin, H.; Lee, B.-H.; Efremov, V.; Lee, S.; Lee, H. S.; Kim, J.; Hooch Antink, W.; Park, S.; Lee, K.-S. J. N. M., Atomic-level tuning of Co-N-C catalyst for high-performance electrochemical H_2O_2 production. *Nat. Mater.***2020,** *19*, 436-442.
(32) Teng, Z.; Zhang, Q.; Yang, H.; Kato, K.; Yang, W.; Lu, Y.-R.; Liu, S.; Wang, C.; Yamakata, A.; Su, C. J. N. C., Atomically dispersed antimony on carbon nitride for the artificial photosynthesis of hydrogen peroxide. *Nat. Catal.* **2021,** *4*, 374-384.
(33) Leng, K.; Zhang, J.; Wang, Y.; Li, D.; Bai, L.; Shi, J.; Li, X.; Zheng, L.; Bai, J.; Qu, Y. J. A. F. M., Interfacial Cladding Engineering Suppresses Atomic Thermal Migration to Fabricate Well‐Defined Dual‐Atom Electrocatalysts. *Adv. Funct. Mater.* **2022**, 2205637.

Table of contents

The resultant NbN_3 single atom catalyst exhibit excellent $2e^-$ ORR activity with a near zero onset overpotential and a high H_2O_2 selectivity over 95%, thanks to its unique local environment of unsaturated Nb-N_3 moieties and adjacent oxygen groups, which optimize the adsorption/desorption strength of pivotal reaction intermediates.